

A Study of the Variation of Geometry of Accretion Flows of Compact Objects through Timing and Spectral Analysis of Their Outbursts

P. S. Pal^{1*} and S. K. Chakrabarti^{1†}

¹*S. N. Bose National Centre For Basic Sciences, Kolkata, 700098, India*

ABSTRACT

Temporal and spectral variations of black hole candidates during outbursts have been reported in several publications. It is well known that during an outburst, source becomes softer in first few days, and then returns to hard states after a few weeks or months. In the present paper, we show variation of Comptonization Efficiency (CE), defined to be the ratio of number of power-law photons and number of soft photons injected to into the Compton cloud, as a function of time in several outbursts. Since power-law photons are generated through inverse-Comptonization of the intercepted soft photons, CE is a measure of geometry of Compton cloud. Our investigation indicates that all outbursts start with a large CE and becomes very small after a few days, when the Compton cloud becomes small enough to intercept any significant number of soft photons. CE returns back to a larger value at the end of outburst. We show co-variation of count rates, frequency of quasi-periodic oscillations (QPOs), photon index and CE and establish a general trend of disk geometry variation during outbursts in all systems under consideration.

Key words: Black Holes, Accretion disk, X-rays, Radiation mechanism.

1 INTRODUCTION

It is well known that black hole accretion flows in a compact binary system typically consist of a Keplerian disk which emits soft or low energy photons and a hot Compton cloud which inverse Comptonizes soft photons into high energy photons (Sunyaev & Titarchuk 1985). When a black hole spectral state changes from hard to soft and vice versa, Compton cloud must change its shape and temperature (Chakrabarti & Titarchuk 1995; Tanaka & Lewin 1995): In a soft state, when the accretion rate in the Keplerian disk is high, Compton cloud is smaller and cooler, while in a hard state, when Keplerian disk rate is very low, Compton cloud is larger and hotter. There are various models of the Compton cloud in the literature, ranging from a hot Corona, magnetic corona, to post-shock region of an accreting low angular momentum flow which surrounds the standard Keplerian disk (Haardt & Maraschi 1991; Wandel & Liang 1991; Esin et al. 1997; Janiuk & Czerny 2000; Merloni & Fabian 2001; Zdziarski et al. 2003; Neilsen et al. 2011; Oshuga et al. 2005; Liu et al. 2005; Chakrabarti & Titarchuk 1995; Chakrabarti & Manickam 2000; Rao et al. 2000a; McClintock & Remillard 2006). Along with spectral variabilities, a black hole candidate shows temporal variations also, which is sometimes quasi-periodic (Muno et al. 1999; Chakrabarti et al. 2008, 2009). There are various explanations of quasi-periodic oscillations in literature ranging from disc-seismology to oscillation of post-shock region (Kato 2005; Axelsson et al. 2005; Chakrabarti & Manickam 2000).

Outburst sources are ideal candidates to study changes in the size of a Compton cloud. This is because object is known to be in a hard state at the beginning of an outburst but in a matter of few days to a few weeks, it changes its states to several other states, thereby giving us a unique opportunity to study size variation of Compton cloud very easily. From

* E-mail: parthasarathi.pal@gmail.com; partha.sarathi@bose.res.in

† chakraba@bose.res.in

the spectral analysis, it appears that following sequence is typically followed by most, if not all, outburst sources: hard \rightarrow hard-intermediate \rightarrow soft-intermediate \rightarrow soft \rightarrow soft-intermediate \rightarrow hard-intermediate \rightarrow hard) (Chakrabarti et al. 2008, 2009; Belloni 2010; Nandi et al. 2012).

Recently, Pal et al. (2011) showed that average size of Compton cloud in the variable source GRS 1915+105 changes in a very well defined way as it transits from one variability class to another. They computed a quantity called Comptonizing Efficiency (CE) which is the ratio of number of power-law photons to the number of blackbody photons in the spectrum at a given instant. They show that CE is very small in softer classes and larger for harder classes. Within some of classes, there are evidences of rise and fall of count rates and spectral slopes in a matter of a few seconds. Since number of hard photons depends on optical depth of Compton cloud, we clearly see a change in optical depth of the Compton cloud in that time scale. Furthermore, we see that one variability class goes to another adjacent class whose CE is nearest.

In the present paper, we study variation of Compton cloud size during outbursts of several black hole candidates. We show that outbursts typically start with a large Comptonization efficiency, i.e., a large sized Compton cloud with a poor soft photon source. In rising phase, this cloud becomes progressively smaller and smaller on a daily basis, till it became minimum when the object went to a soft state. Of course, soft photon source gets stronger (soft photon intensity rises) and as a result, the cloud size shrinks (QPO frequency, assumed to be the oscillating frequency of the cloud, rises). In declining phase of an outburst, the trend is exactly reversed. In this paper, we deal with black hole candidates which exhibited outbursts, such as, H1743-322, GX 339-4, 4U 1543-47, XTE J1118+480, XTE J1859+226, GRO J1655-40 and XTE J1550-564. In the next Section, we briefly discuss the objects of our study. In §3, we present the procedure of our analysis. Here, we compute Comptonization Efficiency (CE) of all these outbursts both in rising and declining phases. We show that CE changes with time very rapidly. In general, softer states were found to have a very low CE and the harder states (at the beginning of rising phase and at the end of declining phase) were found to have a very high CE. In §4, we present results and interpret them using physical models. Finally, in §5, we draw our conclusions.

2 OBJECTS OF OUR STUDY

We consider following outburst sources in the study.

(a) The black hole candidate H1743-322 was first discovered by Ariel in 5 August, 1977 Kaluzienski & Holt (1977). Later, it was precisely located by High Energy Astronomical observatory 1 (HEAO) by Doxsey et al. (1977). This object was classified as a black hole candidate by White & Marshall (1983). In March 2003, an outburst along with an increase of source flux by a factor of 3 (60 mCrab in 15-40 keV energy range), was reported by INTEGRAL where X-Ray properties of a black hole candidate were studied (Revnivtsev et al. 2003). Another outburst, along with increase of source flux from 16 - 160 mCrab in 2-10 keV intensity, was reported by Swank (2004) in July, 2004. Several radio ejections are reported during the 2003 outburst (Rupen et al. 2003). Later, from the ejected plasma, radio and X-ray synchrotron emissions are also reported (Corbel et al. 2005). Distance of the object is 8 kpc (Corbel et al. 2005) and mass is estimated to be $M = 10.0 M_{\odot}$ (Chen et al. 2010; McClintock et al. 2009). Outburst of 2009 was analyzed by Chen et al. (2010). Outbursts of 2008 and other outbursts are analyzed by Coriat et al. (2011) and Jonker et al. (2010). Spectral fitting is done with $n_H = 1.6 \times 10^{22} \text{ cm}^{-2}$ (Capitanio et al. 2009).

(b) GX 339-4 is a stellar mass Galactic Black hole candidate. This black hole candidate was first observed by MIT X-Ray detector of OSO-7 during the survey period between October, 1971 and January, 1973 between 1-60 keV energy range. This LMXB is located at (l,b)=338.93, -4.27 (Markert et al. 1973) with RA = $17^h 02^m 49^s.36$ and dec= $-48^{\circ} 47' 22.8''$ (J2000). Optical observation leads to an estimation of mass function to be around $5.8 \pm 0.5 M_{\odot}$ (Hynes et al. 2003a) and $D = 5.8$ kpc (Hynes et al. 2004). Estimated mass of this object is $7.5 \pm 0.8 M_{\odot}$ (Chen 2011). During RXTE *Rossi X-Ray Timing Explorer* Era, GX 339-4 had undergone several outburst phases (1998, 2002/2003, 2004/2005, 2006/2007, 2010). GX 339-4 was observed several times by RXTE during outburst period (Del Santo et al. 2009; Motta et al. 2009). In 2006, Krimm et al. (2006) reported beginning of 2007/2007 outburst of GX 339-4 with increase of source flux to 230 mCrab in 15-50 keV energy range by Swift-BAT. In 2010, Yamaoka et al. (2010) reported an increase in source flux from 17 mCrab to 26 ± 5 mCrab in 4-10 keV energy range for GX 339-4. In the present paper, we will analyze data of 2006/2007 and 2010 outbursts. For spectral analysis, $n_H = 0.5 \times 10^{22} \text{ cm}^{-2}$ is taken towards this source (Mendez & Van der Klis 1997; Kong et al. 2000).

(c) Black hole candidate 4U 1543-47 was discovered on August 17, 1971 by Uhuru satellite (Matilsky et al. 1972). Since discovery, X-ray outbursts have been observed in 1983, 1992, 2002. Optical observation was found by Blissett et al. (1983) during 1983 outburst. The 2002 outburst commenced on MJD 52442 along with increase in source flux from 0.054 to 1.65 mCrab in 2-12 keV energy range and was observed simultaneously in X-rays by RXTE (Miller & Remillard 2002; Park et al. 2004) in Radio by Molonglo Observatory Synthesis Telescope (MOST) (Hunstead & Webb 2002; Park et al. 2004) in Optical and Infrared by YALO Telescope (Buxton & Bailyn 2004). Several multi-wave length observations are reported for 2002 outburst of 4U 1543-47 (Kalemci et al. 2005). The blackhole mass $9.4 \pm 0.2 M_{\odot}$, $D=7.5 \pm 1.0$ kpc, $i=20.7 \pm 1.0^{\circ}$ was reported

by Park et al. (2004). Fourier resolved spectroscopy is also carried out for the source during this outburst (Reig et al. 2006). For spectral analysis, interstellar absorption is taken to be $n_H = 4.0 \times 10^{21} \text{ cm}^{-2}$ (Dickey & Lockman 1990; Park et al. 2004).

(d) XTE J1118+480 was first discovered by All Sky Monitor (ASM) by Remillard et al. (2000) in March, 2000, while Garcia et al. (2000) spectroscopically observed its optical counter part. This object is observed simultaneously in optical, and infrared to determine the physical parameters of the black hole (Gelino et al. 2006). The orbital inclination angle is $68^\circ \pm 2^\circ$. This angle corresponds to a primary black hole mass of $8.53 \pm 0.60 M_\odot$. Distance of the black hole is 1.72 ± 0.10 kpc. This object has shown outbursts in 2000 (Hynes et al. 2000; McClintock et al. 2001; Chaty et al. 2003) and 2005 (Hynes et al. 2006; Remillard et al. 2005; Pooley 2005; Rupen et al. 2005; Zurita et al. 2005a,b, 2006). Several authors have discussed disk-jet connection of this compact object (Kanbach et al. 2001; Hynes et al. 2003b) to explain source high energy photons (Markoff et al. 2001; Yuan et al. 2005). Remillard et al. (2005) reported this outburst as a faint x-ray outburst as the source flux increases from 15-19 mCrab in 2-12 keV energy band. Optical (Zurita et al. 2005a,b, 2006) and radio (Pooley 2005; Rupen et al. 2005) counter parts have also been observed. Spectral fitting is done with $n_H = 1.3 \times 10^{20} \text{ cm}^{-2}$ (Brocksopp et al. 2010).

(e) X-Ray transient XTE J1859+226 was discovered by the All Sky Monitor (ASM) onboard RXTE on 9 October, 1999 (Wood et al. 1999). Smith (1999) reported the increase of source flux up to 1.37 mCrab in 2-12 keV energy range. Mass and inclination angle are $4.5 \pm 0.6 M_\odot$ and 70° respectively (Corral-Santana et al. 2011). Distance of the compact object is 11 kpc (Zurita et al. 2002). Spectral analysis is done with $n_H = 2.21 \times 10^{21} \text{ cm}^{-2}$ (Dickey & Lockman 1990).

(f) X-Ray Nova GRO J1655-40 was first discovered by BATSE onboard Compton Gamma Ray Observatory on 1994 July, 27 (Zhang et al. 1994). Optical counter-part was discovered by Bailyn et al. (1995). Mass and inclination angle are $M = 7.02 \pm 0.22 M_\odot$, $\theta = 69^\circ.5 \pm 0^\circ.1$ (Orosz & Bailyn 1997; Van der Hooft et al. 1998) respectively. Distance of the compact object is 3.2 ± 0.2 kpc (Hjellming & Rupen 1995). In the last week of February, 2005, this source became active as the source flux increased from 0.3 mCrab to 4.1 mCrab in 2-10 keV energy range (Markwardt & Swank 2005) and outburst continued for 260 days (Shaposhnikov et al. 2007). Before this, several outbursts were reported of the same source (Sobczak et al. 1999b). Hydrogen column density is fixed at $0.89 \times 10^{22} \text{ cm}^{-2}$ (Zhang et al. 1997).

(g) X-Ray transient XTE J1550-564 was first discovered by ASM in 1998 September 7 (Smith 1998) and by CGRO (Wilson et al. 1998). Optical (Orosz et al. 1998b) and radio (Campbell-Wilson et al. 1998) counterparts are detected shortly after this. Optical photometry reveals a binary period of 1.541 ± 0.009 days (Jain et al. 2001) during the 1998 outburst. During this outburst, presence of a superluminal jet is observed along with the massive X-Ray flare (Hannikainen et al. 2001). Later observations revealed that the black hole has a mass of $10.0 \pm 1.5 M_\odot$ and the companion star is a late-type subgiant (G8IV-K4III). Binary inclination angle is $72^\circ \pm 5^\circ$ (Orosz et al. 2002). Distance of the black hole is 6 kpc (Sobczak et al. 1999a). In 1998, luminosity of the compact object is reported to be 6.8 Crab in 2-12 keV energy range (Rutledge et al. 1998). Interstellar absorption $n_H = 0.85 \times 10^{22} \text{ cm}^{-2}$ is taken (Tomsick et al. 2001a).

3 ANALYSIS PROCEDURE

In this paper, we analyzed RXTE data and results are summarized in Table: 1. We chose data sets by MJDs of outbursts obtained from literature. These data are downloaded from HEASARC, NASA Archive. During analysis, we exclude data collected for elevation angles less than 10° , for offset greater than 0.02° and those acquired during the South Atlantic Anomaly (SAA) passage. We selected PCU2 data as it was active most of the time. Here we calculated 3.0 – 40.0 keV counts in kcts/s and plot them in top panels of Figs. 1-4 described below. Power Density Spectrum (PDS) is generated by standard FTOOLS task “powspec” with a suitable normalization. Data is binned in 0.01s to obtain a Nyquist frequency of 50 Hz as power beyond this is found to be insignificant. PDSs are normalized to give squared *rms* fractional variability per Hertz. Evolution of QPO frequency is plotted in second panel from top of Figs. 1-4.

3.1 Spectral Analysis

Spectral analysis of RXTE PCA data is done by using “standard2” mode data which have 16 sec time resolution. We constrained our energy selection from 3.0 keV to 40 keV from the observational data. Source spectrum is generated using FTOOLS task “SAEXTRACT” with 16 sec time bin from “standard2” data. Background fits file is generated from “standard2” fits file by FTOOLS task “runpcabackest” with standard FILTER file provided with the package. Background source spectrum is generated using FTOOLS task “SAEXTRACT” with 16 sec time bin from background fits file. Standard FTOOLS task “pcarsp” is used to generate response file with appropriate detector information. Exposure time is corrected for source and background spectra with deadtime correction factor. Spectral analysis and modeling was performed using XSPEC (V.12) astrophysical fitting package. For model fitting of PCA spectra, we have used a systematic error of 0.5%. Spectra are fitted with *diskbb* and *power-law* model along with hydrogen column density for absorption. We use *Gaussian* for iron line as required for best fit. During fitting of spectra we adopted a technique introduced by Sobczak et al. (1999b); Pal et al. (2011, 2013),

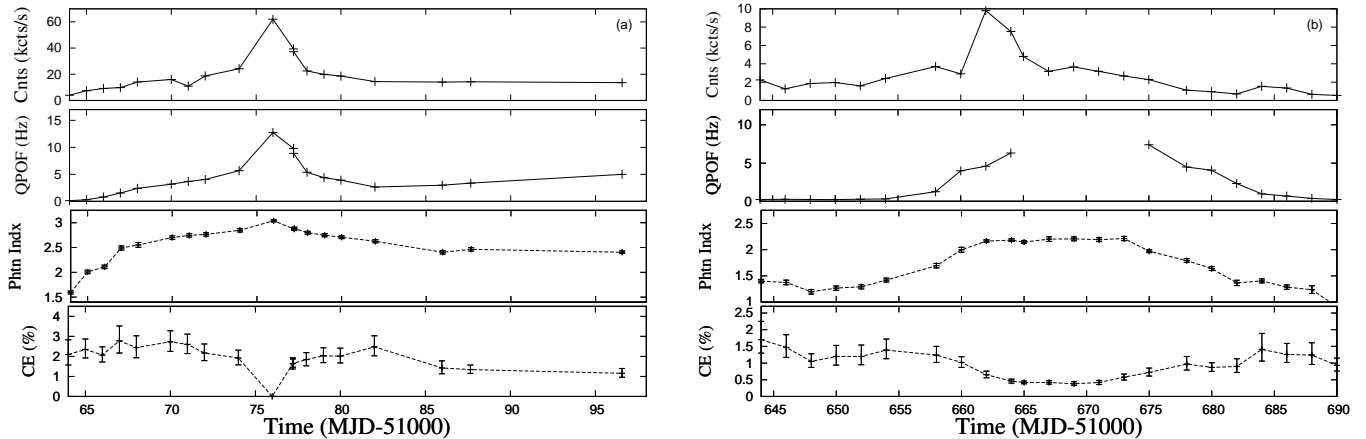


Figure 1. Simultaneous variation of 2.0 – 40.0 keV counts in kcts/s (upper panel), QPO frequency in Hz (second panel), spectral slope (third panel) and the CE (lower panel) of (a) XTE J1550-564 during its 1998 outburst and (b) XTE J1550-564 during its 2000 outburst.

to obtain spectral parameters. We calculated error-bars at 90% confidence level in each case. Morrison & McCammon (1983) reported that interstellar absorption mainly affects photons from 0.03 to 10.0 keV. It is important to consider this effect in RXTE analysis since we need to count injected soft photons up to 10.0 keV as accurately as possible. We chose n_H as appropriate for each candidate to take care of this effect.

3.2 Efficiency of Comptonization

In the literature, usual trend is to plot hardness ratio HR (say, the ratio of 6-40 keV photons divided by 2-6 keV photons) when it comes to understand how important Compton scattering is. However, there are several problems in this definition: (a) HR does not depend on mass of the black hole, although hard (Comptonized) and soft photons change their meaning with the mass of the black hole. For instance, soft photons in lower mass case could be Comptonized photons in higher mass case. Thus HR cannot be compared for two objects, or even in two episodes of the same object. To circumvent this problem, we define a new parameter (Pal et al. 2011, 2013) called Comptonization Efficiency (CE) which is defined purely on physical ground and independent of any model or mass of the black hole. Since for stellar mass black holes we expect peak radiation from standard Keplerian disk to be at around 0.5 – 1 keV, and slope of power-law tail is defined for 2 – 10 keV region, we choose a range 0.1 – 40 keV to define CE, both ends being far from the expected values. We compute total number of soft (seed) photons (N_{BB}) from Keplerian disk from multicolour black body and total number of power-law photons (N_{PL}) in ranges dynamically determined by best fits obtained after correcting observational data using energy dependent absorption due to hydrogen column. Since these ranges are obtained dynamically, the ratio $CE = N_{PL}/N_{BB}$ is independent of mass of a black hole or any specific model of accretion flow. Hence CE of two different objects can be compared, which we do in this paper. Number of black body photons are obtained following Makishima et al. (1986). Here we count the photons within the energy range starting from 0.1 keV to the best fitted upper energy limit dbb_e by first fitting the spectrum with diskbb model alone (Sobczak et al. 1999b). Upper limit of black body energy dbb_e is obtained from the consideration that the reduced χ^2 value from resultant fit should be ~ 1.0 . This upper limit may vary with time and from one data set to another.

Comptonized photons N_{PL} are calculated by using the power-law equation given below,

$$P(E) = N(E)^{-\alpha}, \quad (1)$$

where, α is the power-law index and N is the total photons/s/keV at 1 keV. It is reported in Titarchuk (1994), that the Comptonization spectrum will have a peak at around $3 \times T_{in}$, where, T_{in} is the temperature at the inner edge of the standard disk. Thus, the power-law is integrated from $3 \times T_{in}$ to 40 keV to calculate total rate of Comptonized photons (photons/s). T_{in} and α comes from spectral fit of each data. Here we assume that the black hole is non-rotating. For rotating flows the corresponding spectral properties of the standard disk has to be used.

4 RESULTS & DISCUSSION

Observation IDs of data sets analyzed in this paper are given in Table: 1. In Table: 2, spectral fitting parameters of sample datasets are shown. Error-bars are calculated at 90% confidence level in each case. To ease discussion, we keep two component advective flow (TCAF) model of Chakrabarti & Titarchuk (1995) in the back of our mind. Of course, our result does not

Object	Outburst	Analysis Time	Obs ID
XTE J1550-564	1998	08/09/1998	30188-06-03-00, 30188-06-01-00 30188-06-01-02 30188-06-04-00
		to 10/10/1998	30188-06-05-00, 30188-06-07-00, 30188-06-09-00, 30188-06-11-00 30191-01-01-00, 30191-01-02-00, 30191-01-05-00, 30191-01-06-00 30191-01-08-00, 30191-01-09-00, 30191-01-10-00, 30191-01-13-00, 30191-01-16-00, 30191-01-18-01, 30191-01-27-00
XTE J1550-564	2000	10/04/2000	50137-02-01-00, 50137-02-02-00, 50137-02-03-00, 50137-02-04-00,
		to 26/04/2000	50137-02-05-00, 50137-02-06-00, 50134-02-01-00, 50134-02-01-01, 50134-02-02-00, 50134-02-03-00, 50134-02-03-01, 50134-02-04-00, 50134-02-05-00, 50134-02-07-01, 50134-01-01-00, 50134-01-03-00, 50134-01-05-00, 50135-01-01-00, 50135-01-02-00, 50135-01-04-00, 50135-01-05-00, 50135-01-07-00, 50135-01-08-00
GX 339-4	2007	28/12/2006	92052-07-04-00, 92052-07-05-00, 92428-01-01-00, 92052-07-06-00,
		to 26/05/2007	92052-07-06-01, 92428-01-02-00, 92428-01-03-00, 92035-01-01-02, 92035-01-02-00, 92035-01-02-08, 92035-01-03-01, 92428-01-04-04, 92035-01-04-02, 92085-01-01-06, 92085-01-02-03, 92085-01-02-06, 92085-01-03-02, 92085-01-04-13, 92085-01-04-02, 92085-02-01-01, 92085-02-01-04, 92085-02-02-00, 92085-02-02-01, 92085-02-03-00, 92085-02-03-01, 92085-02-04-00, 92085-02-04-02, 92085-02-05-01, 92085-02-05-02, 92704-03-02-00, 92704-03-03-00, 92704-03-05-01, 92704-03-07-01, 92704-03-09-02, 92704-03-11-01 92704-03-13-02, 92704-03-15-00
GX 339-4	2010	18/01/2010 to 08/05/2010	95409-01-02-01, 95409-01-07-01, 95409-01-10-03, 95409-01-13-04, 95409-01-14-04, 95409-01-15-01, 95409-01-15-02, 95409-01-15-04 95409-01-15-06, 95409-01-16-00, 95409-01-16-03, 95409-01-17-01, 95409-01-17-03, 95409-01-17-05, 95409-01-18-00, 95335-01-01-00
H 1743-322	2008	16/01/2008 to 04/02/2008	93427-01-01-00, 93427-01-02-01, 93427-01-02-02, 93427-01-03-00, 93427-01-03-01, 93427-01-03-04, 93427-01-04-01, 93427-01-04-02
H 1743-322	2009	29/05/2009 to 07/07/2009	94413-01-02-00, 94413-01-02-02, 94413-01-02-05, 94413-01-02-03 94413-01-03-00, 94413-01-03-01 94413-01-03-04, 94413-01-04-00, 94413-01-04-04, 94413-01-07-01
XTE 1859+226	2000	12/10/1999	40124-01-05-00, 40124-01-09-00, 40124-01-12-00, 40124-01-17-00,
		to 26/02/2000	40124-01-20-00, 40124-01-23-01, 40124-01-29-00, 40124-01-33-01, 40124-01-38-01, 40124-01-44-00, 40122-01-04-00, 40124-01-54-00, 40124-01-55-03, 40124-01-57-01, 40124-01-58-01, 40124-01-59-00, 40124-01-60-00, 40124-01-61-00, 40124-01-62-00, 40124-01-63-01, 40124-01-64-01, 40124-01-65-00, 40124-01-66-00, 40440-01-01-00, 40440-01-02-00, 40440-01-03-00
XTE 1118+480	2005	13/01/2005	90111-01-01-00, 90011-01-01-00, 90011-01-01-02, 90011-01-01-09,
		to 26/01/2005	90011-01-01-11, 90011-01-01-06, 90111-01-02-03, 90111-01-02-07, 90111-01-02-10, 90111-01-02-11
GRO J1655-40	2005	06/03/2005	91404-01-01-01, 91404-01-01-04, 91702-01-01-03, 91702-01-01-05
		to 19/09/2005	90704-04-01-01, 90704-04-01-00, 91702-01-02-00, 91702-01-02-01 91702-01-02-03, 91702-01-13-00, 91702-01-19-00, 91702-01-29-00 91702-01-36-01, 91702-01-44-03, 91702-01-44-01, 91702-01-44-04 91702-01-52-02, 91702-01-56-03, 91702-01-60-00, 91702-01-63-00 91702-01-68-01, 91702-01-70-00, 91702-01-72-02, 91702-01-77-00 91702-01-78-01, 91702-01-83-01, 91702-01-85-00, 91702-01-90-02 91702-01-94-00, 91702-01-95-02, 91702-01-01-10, 91702-01-05-11 91702-01-16-10, 91702-01-24-10, 91702-01-29-10, 91702-01-33-11 91702-01-41-11, 91702-01-50-10, 91702-01-51-13, 91702-01-74-00 91702-01-76-00, 91702-01-79-00, 91702-01-80-00, 91702-01-80-01
4U1543-47	2002	17/06/2002 to 25/07/2002	70133-01-01-00, 70133-01-02-00, 70133-01-04-00, 70132-01-01-00 70133-01-12-00, 70133-01-07-00, 70133-01-10-00 70133-01-15-00, 70133-01-18-00, 70133-01-20-00, 70133-01-26-00 70133-01-28-00, 70133-01-31-00, 70124-02-03-00

Table 1. Observation IDs analyzed in this paper.

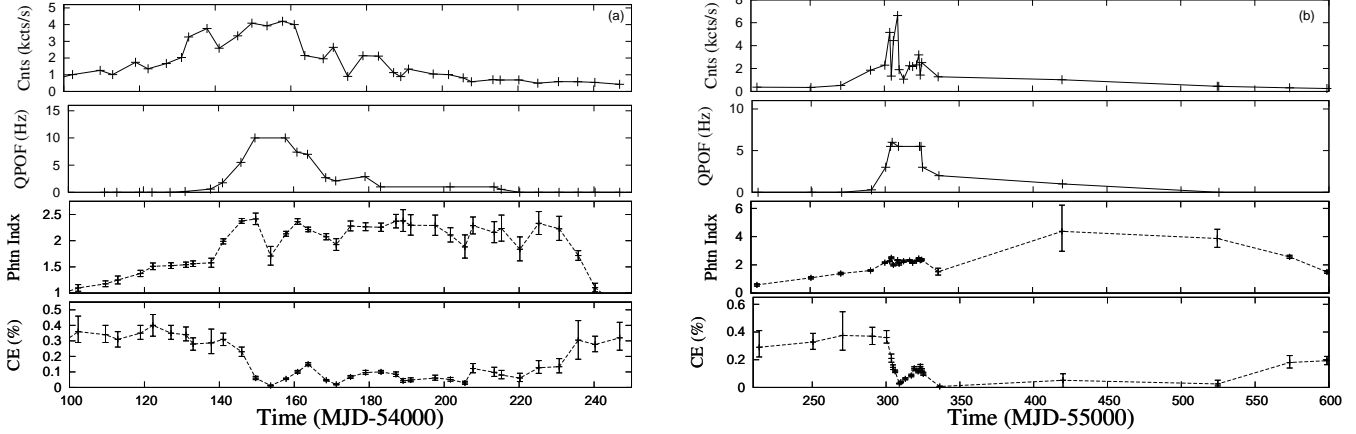


Figure 2. Same as in Fig. 1, except (a) GX 339-4 during its 2007 outburst and (b) GX 339-4 during its 2010 outburst.

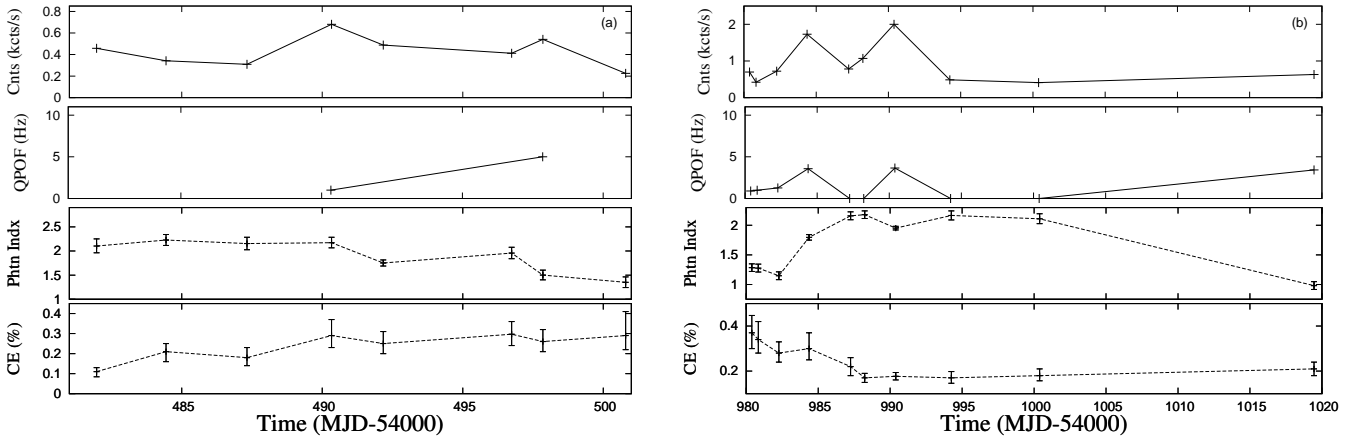


Figure 3. Same as in Fig. 1, except (a) H 1743-322 during its 2008 outburst (b) H 1743-322 during its 2009 outburst.

depend on any specific model, as long as there are sources of seed photons and hot electrons for inverse Comptonization of these seed photons.

4.1 XTE J1550-564

Outbursts of 1998 and 2000 of Galactic black hole XTE J1550-564 are analyzed in this paper. 1998 outburst is analyzed from MJD 51064 (08/09/1998) to MJD 51097 (10/10/1998). Result is shown in Fig. 1a. Chakrabarti et al. (2009) reported that QPO was always observed and thus the oscillating shock in so-called ‘propagating’ shock model (Debnath et al. 2010) does not disappear behind the horizon or the shock does not become weak enough. The post-shock region is known as the CENTrifugal pressure supported BOundary Layer or the CENBOL. It is the Compton cloud in the two component advective flow (TCAF) model (Chakrabarti & Titarchuk 1995). In initial stages of the outburst, CE was around 2 – 3%. CE gradually dropped to $\sim 0.001\%$ as peak of outburst is reached and photon index became highest. Physically, this means a gradual decrease of size of CENBOL as Keplerian disk rate rises and cools CENBOL down. After the peak, CE started to increase to 2 – 3% in the decline phase, though it finally converged to $\sim 1\%$. Variation of QPOs during this outburst is discussed in details in Chakrabarti et al. (2009).

We then analyzed 2000 outburst of the same source from MJD 51644 (10/04/2000) to MJD 51690 (26/05/2000). Result is shown in Fig. 1b. Light curve looks qualitatively the same as that of the 1998 outburst. During this outburst, CE varies initially between 1.0 – 1.5% but after MJD 51660, CE is reduced to less than 0.5%. This indicates that oscillating shock was still present. After a few days, CE again increased to $\sim 1.5\%$ before settling to a $\sim 1\%$. As the shock recedes from the black hole, optical depth initially rises, but then goes down as CENBOL density drops rapidly. This may be the cause for CE to rise first and then to come down at $\sim 1\%$ in both outbursts.

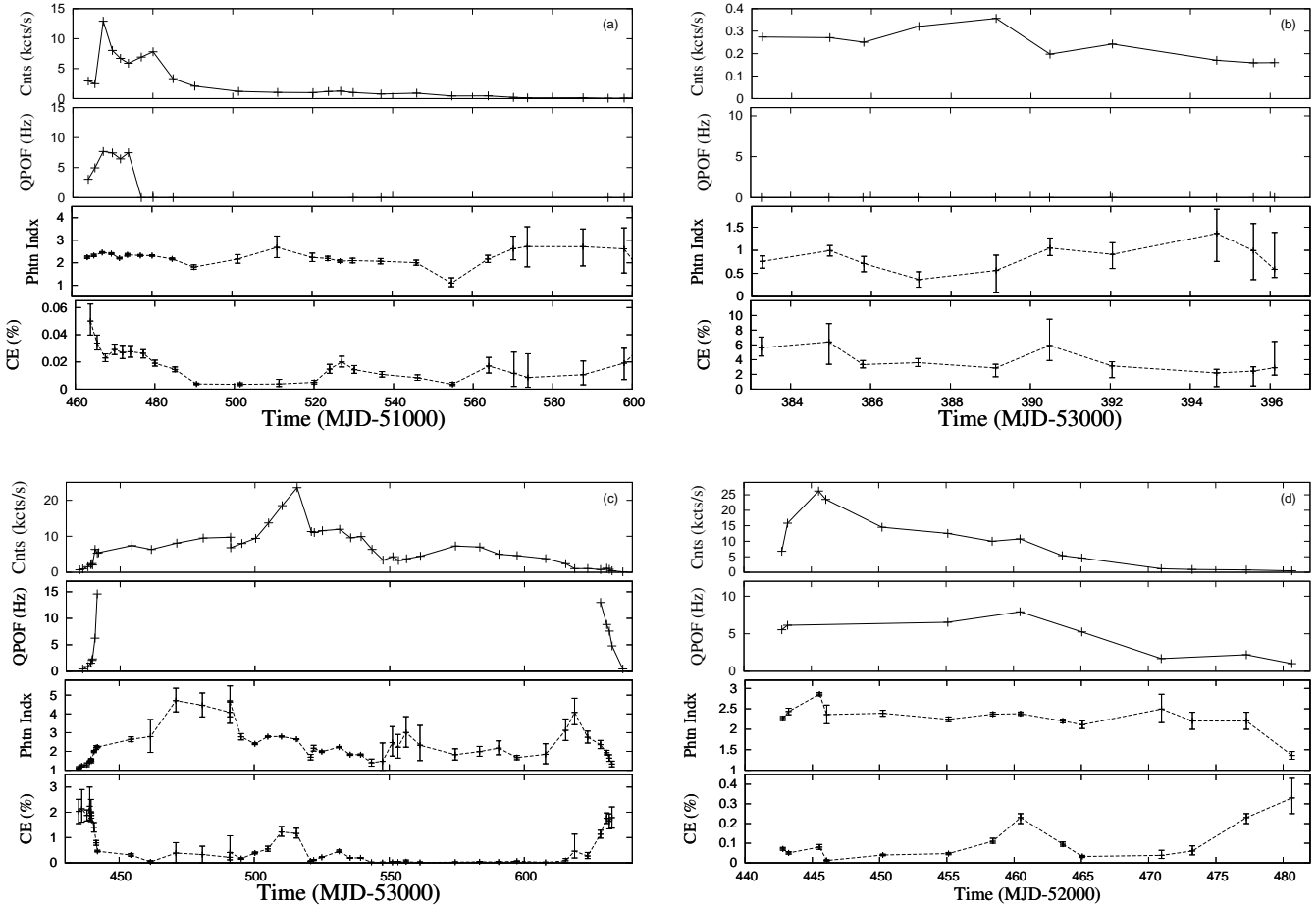


Figure 4. Same as in Fig. 1, except (a) XTE 1859+226 during its 2000 outburst, (b) XTE 1118+480 during its 2005 outburst, (c) GRO J1655-40 during its 2005 outburst and (d) 4U 1543-47 during its 2002 outburst.

4.2 GX 339-4

We analyzed 2007 and 2010 outbursts of GX 339-4. 2007 outburst is analyzed from MJD 54097 (28/12/2006) to MJD 54247 (26/05/2007). Result is shown in Fig. 2a. During initial stage of rising phase, CE remained roughly constant at $\sim 0.3 - 0.4\%$ for about 40 days. Constancy of CE may mean that while CENBOL is getting smaller, density is becoming larger and thus optical depth remains roughly constant to intercept roughly similar number of soft photons. After that, CE decreased sharply when the CENOBOL disappeared. A sporadic shock is formed during soft and hard-intermediate states, raising CE. QPO remained absent for the next 80 days when CE varied between $\sim 0.05 - 0.1\%$. After that, CE is increased to $\sim 0.3\%$, close to its initial value.

2010 outburst is analyzed from MJD 55214 (18/01/2010) to MJD 55324 (08/05/2010). Result is shown in Fig. 2b. During initial phase, CE remained constant at around 0.3% for 80 days. After that CE decreases sharply below 0.1% .

4.3 H 1743-322

We analyzed outbursts of 2008 and 2009 of H 1743-322. 2008 outburst is analyzed from MJD 54482 (16/01/2008) to MJD 54500 (04/02/2008). Only declining phase is observed by RXTE for this outburst. Result is shown in Fig. 3a. Observation started when the object is in a softer state having a high photon index. CE also started from a minimum value of $\sim 0.1\%$. Eventually, at the end of the outburst, CE increased to the high state value of $\sim 0.3\%$.

2009 outburst is analyzed from MJD 54980 (29/05/2009) to MJD 55019 (07/07/2009). During rising phase, CE decreased from $\sim 0.4\%$ to 0.15% within 10 days. During declining phase, CE rises very slowly 0.2% . Result is shown in Fig. 3b. In this case also, near constancy of CE indicates that optical depth is nearly constant even through shock wave is receding as is obvious from time variation of QPOs (Chakrabarti et al. 2008, 2009; Nandi et al. 2012).

Compact Object (Outburst)	Time MJD	QPO Hz	T_{in} (keV)	dbb_e (keV)	χ^2 (dofs)	Soft Phtns kphntns/s	Power-law index	χ^2 (dofs)	Hard Phtns (kphntns/s)	CE (%)
XTE J1550-564(1998)	51065	0.3	$1.74^{+0.10}_{-0.09}$	4.75	1.5(7)	$43.89^{+8.15}_{-8.46}$	$2.00^{+0.03}_{-0.03}$	1.3(71)	$1.03^{+0.04}_{-0.04}$	$2.35^{+0.52}_{-0.43}$
XTE J1550-564(2000)	51648	0.2	$1.60^{+0.14}_{-0.12}$	6.0	1.7(8)	$5.27^{+0.10}_{-0.08}$	$1.19^{+0.04}_{-0.04}$	1.5(74)	$0.06^{+0.001}_{-0.001}$	$1.05^{+0.23}_{-0.18}$
XTE J1550-564(2000)	51665	-	$1.02^{+0.02}_{-0.02}$	8.5	1.4(9)	$130.71^{+9.9}_{-10.0}$	$2.14^{+0.03}_{-0.03}$	0.9(69)	$0.55^{+0.02}_{-0.01}$	$0.42^{+0.04}_{-0.04}$
GX 339-4(2007)	54141	1.7	$1.85^{+0.06}_{-0.05}$	5.75	1.36(8)	$49.38^{+4.6}_{-4.1}$	$1.99^{+0.05}_{-0.05}$	1.6(74)	$0.15^{+0.006}_{-0.005}$	$0.31^{+0.04}_{-0.04}$
GX 339-4(2007)	54158	10.0	$0.91^{+0.01}_{-0.01}$	8.5	1.8(10)	$574.41^{+21.10}_{-20.14}$	$2.13^{+0.05}_{-0.04}$	0.9(74)	$0.32^{+0.02}_{-0.01}$	$0.06^{+0.004}_{-0.003}$
GX 339-4(2010)	55291	0.3	$1.54^{+0.11}_{-0.10}$	6.0	0.98(9)	$24.49^{+3.86}_{-3.15}$	$1.60^{+0.05}_{-0.05}$	1.2(79)	$0.09^{+0.003}_{-0.003}$	$0.37^{+0.06}_{-0.06}$
GX 339-4(2010)	55313	-	$0.93^{+0.01}_{-0.01}$	8.5	0.98(10)	$186.29^{+7.53}_{-7.15}$	$2.26^{+0.08}_{-0.08}$	1.1(79)	$0.11^{+0.01}_{-0.009}$	$0.06^{+0.08}_{-0.07}$
H 1743-322(2008)	54498	5.0	$1.61^{+0.08}_{-0.07}$	5.75	1.2(8)	$11.12^{+1.8}_{-1.5}$	$1.5^{+0.1}_{-0.1}$	0.99(79)	$0.03^{+0.002}_{-0.001}$	$0.26^{+0.06}_{-0.05}$
H 1743-322(2009)	54990	3.65	$1.18^{+0.03}_{-0.02}$	5.25	0.7(9)	$136.00^{+9.69}_{-8.84}$	$1.95^{+0.03}_{-0.03}$	1.5(79)	$0.24^{+0.006}_{-0.006}$	$0.18^{+0.02}_{-0.02}$
XTE J1859+226(2000)	51464	3.0	$1.32^{+0.08}_{-0.07}$	5.5	1.1(9)	$668.59^{+130.78}_{-103.10}$	$2.24^{+0.06}_{-0.06}$	1.6(79)	$0.33^{+0.02}_{-0.02}$	$0.05^{+0.01}_{-0.01}$
XTE J1859+226(2000)	51480	-	$1.11^{+0.03}_{-0.03}$	7.5	0.8(8)	$3832.64^{+320.66}_{-288.11}$	$2.32^{+0.03}_{-0.03}$	1.1(75)	$0.73^{+0.03}_{-0.02}$	$0.02^{+0.002}_{-0.002}$
XTE J1118+480(2005)	53395	-	$1.05^{+0.05}_{-0.04}$	6.5	0.94(9)	$312.01^{+47.95}_{-39.70}$	$2.75^{+0.03}_{-0.03}$	1.6(75)	$6.33^{+0.28}_{-0.26}$	$2.20^{+0.40}_{-0.34}$
GRO J1655-40(2005)	53439	1.5	$1.54^{+0.17}_{-0.13}$	5.75	0.9(7)	$4.36^{+1.37}_{-0.95}$	$1.46^{+0.03}_{-0.03}$	1.3(75)	$0.10^{+0.002}_{-0.002}$	$2.24^{+0.7}_{-0.5}$
GRO J1655-40(2005)	53591	-	$1.05^{+0.003}_{-0.003}$	10.0	0.8(11)	$111.56^{+1.19}_{-1.17}$	$2.17^{+0.39}_{-0.35}$	1.2(79)	$0.04^{+0.02}_{-0.02}$	$0.03^{+0.02}_{-0.02}$
4U 1543-47(2005)	52460	7.9	$1.03^{+0.02}_{-0.02}$	5.5	1.6(7)	$401.31^{+30.17}_{-27.43}$	$2.38^{+0.04}_{-0.04}$	1.3(79)	$0.91^{+0.05}_{-0.04}$	$0.23^{+0.02}_{-0.03}$

Table 2. Parameters for spectral fits of sample dataset with diskbb plus power-law models. T_{in} is black body temperature obtained from fitting. dbb_e is upper limit energy of disk blackbody spectrum. ‘Soft’ column gives blackbody photons in $0.1 - dbb_e$ keV. The column ‘power-law’ contains power-law index α obtained from our fitting. Column ‘hard photons’ contains rate at which Comptonized photons are emitted in the range $3 \times T_{in}$ to 40 keV. CE is Comptonizing efficiency.

4.4 XTE 1859+226

We analyzed 2000 outburst of XTE 1859+226. Compact object is analyzed from MJD 51463 (12/10/1999) to MJD 51600 (26/02/2000). Result of analysis is shown in Fig. 4a. During onset phase, CE dropped sharply from $\sim 0.06\%$ to 0.003% within 30 days. After that, CE remained low for around 20 days. There is a bumps in CE at around MJD 53510, and they could be due to higher accretion rates causing the CENBOL to swell by radiation pressure. In the last phase, CE returned back to pre-burst value corresponding to a hard state. During this outburst, QPO frequency increased gradually from 3 Hz to 7.5 Hz from MJD 51463 to 51473, i.e., within 10 days. After that, QPOs did not reappear.

4.5 XTE 1118+480

We analyzed 2005 outburst of XTE 1118+480 and result is shown in Fig. 4b. Data is from MJD 53383 (13/01/2005) to MJD 53396 (26/01/2005). During this outburst, CE was varying between 3% and 6%. In not too many days QPOs were observed during the outburst (Remillard et al. 2005).

4.6 GRO J1655-40

We analyzed 2005 outburst of GRO J1655-40 and result shown in Fig. 4c. The compact object is analyzed from MJD 53435 (06/03/2005) to MJD 53632 (19/09/2005). During this outburst CE was varying between 2% and 0.1%. QPO variation is already reported in Chakrabarti et al. (2008).

4.7 4U 1543-47

We analyzed 2002 outburst of 4U 1543-47 and results are shown in Fig. 4d. Compact object is analyzed from MJD 52442 (17/06/2002) to MJD 52480 (25/07/2002). Here CE varies between 0.3% to 0.01%. In case of this outburst, QPO is increased from 5 to 8 Hz from MJD 52442 to MJD 52460, then decreased to 1 Hz from MJD 52460 to MJD 52480.

Compact Object	Outburst (Year)	Mass ($\approx M_{\odot}$)	CE_{min} (%)	CE_{max} (%)	L_{min} (L_{Edd})	L_{max} (L_{Edd})	QPO_{min} (Hz)	QPO_{max} (Hz)
XTE J1550-564	1998	9.6	0.0011	2.78	0.26	1.8	0.3	12.7
XTE J1550-564	2000	9.6	0.4	1.7	0.01	0.17	0.3	6.3
GX 339-4	2007	7.5	0.02	0.4	0.006	0.26	0.6	10.0
GX 339-4	2010	7.5	0.03	0.375	0.007	0.16	0.3	6.0
H 1743-322	2008	10.0	0.1	0.3	0.01	0.04	1.0	5.0
H 1743-322	2009	10.0	0.17	0.37	0.02	0.18	1.0	3.7
XTE J1859+226	2000	4.5	0.004	0.05	0.01	0.20	3.0	7.6
XTE J1118+480	2005	8.5	2.2	6.4	0.0003	0.001	-	-
GRO J1655-40	2005	7.02	0.011	2.24	0.003	0.22	0.4	8.0
4U 1543-47	2002	9.4	0.012	0.33	0.01	0.59	1.0	8.0
GRS 1915+105	-	14	0.005	0.8	0.8	1.4	3.0	10.0

Table 3. Variation of CE, Luminosity and QPO for different compact objects during their outbursts. Data for GRS 1915+105 is presented for comparison.

5 SUMMARY OF RESULTS AND A COMPARISON WITH GRS 1915+105

In Table: 3, we summarize results of our analysis. Maximum and minimum values of CE, luminosity, QPO frequency, and mass of compact objects are put together. It is instructive to compare results with those obtained for a highly variable black hole candidate GRS 1915+105 (Pal et al. 2011, 2013) which is believed to be in a soft-intermediate state of some long duration outburst. Thus, Table: 3 also gives results of this source. Since CE is defined in a way to eliminate the effects of the mass, our comparison is meaningful, even when the mass varies by a factor of more than three. In GRS 1915+105, CE varies strongly with a low value for generally softer classes, to a high value for generally harder classes. We clearly note that CE of GRS 1915+105 varies from 0.005 to 0.8, both ends being far from extreme values. These numbers indicate that if GRS 1915+105 underwent an outburst long ago, it is still in a soft-intermediate state. The CE of GRS 1915+105 was found to be very meaningful since occurrence of variability class transitions of this object follows the sequence of increasing or decreasing CE (Pal et al. 2013).

6 DISCUSSIONS & CONCLUSIONS

In this paper, we analyzed several black hole candidates which exhibit outbursts and shown the time dependence of Comptonizing efficiency, QPOs and the spectral index. We tried to understand the results using the TCAF model of (Chakrabarti & Titarchuk 1995) and its time varying form, namely, propagatory oscillating shock (POS) model of the outbursts (Chakrabarti et al. 2008, 2009; Dutta & Chakrabarti 2010; Debnath et al. 2010), though any model which relies on soft photons and inverse Comptonization would be fine, since CE depends on the ratio of Comptonized photons and soft seed photons. In TCAF model, a standard Keplerian disk is surrounded by a faster moving low-angular momentum flow (sub-Keplerian) which produces a centrifugal pressure supported shock where the flow is puffed up and produces the so-called Compton cloud to inverse Comptonize intercepted soft photons coming from the Keplerian disk. Oscillation of post-shock region or CENBOL causes low frequency QPOs in black hole candidates.

In the backdrop of this model, our goal is to study how the optical depth of the CENBOL changes with time in a generic outburst source. If we had computed hardness ratio or HR, where the soft and hard photons are counted using the same fixed energy bins, a comparison of its behavior from one object to another would not be possible. This is because seed photons of one black hole could be Comptonized photon for another. On the other hand, CE as defined by us characterizes soft and hard photons objectively and as such does not depend on mass of the black hole or its accretion rate. Thus a comparison is possible. It is true that we restrict ourselves from 0.1 to 40 keV photons. However, for stellar mass black holes, these boundary values are far away from relevant energies in which respective photons are important.

We came to a conclusion that generally speaking, all outbursts start and end with a large Compton cloud size, though not necessarily with the highest optical depth. As the outburst progresses, CE becomes minimum at peak of an outburst i.e., size of CENBOL becomes very small. We find that CE in outburst sources may vary from almost ~ 0.0 to $\sim 3\%$. In contrast, variable source GRS 1915+105 has CE between 0.005 to 0.8 and has relatively high luminosity (even after factoring out effects

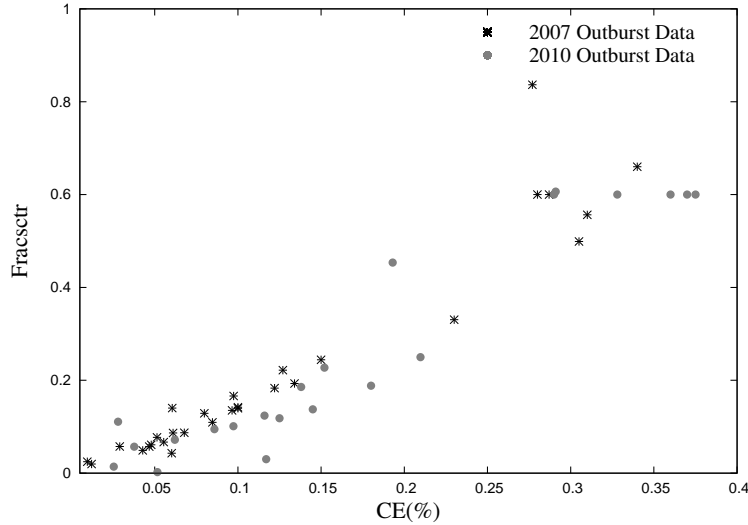


Figure 5. Variation of fracsctr with CE(%) for 2007 and 2010 outbursts of GX 339-4 data. Black stars and gray circle points respectively represent data of 2007 and 2010 outbursts. This plot shows variation of fracsctr with CE(%) computed in 0.1-40 keV range.

of mass of the black hole), suggesting that it is in a soft-intermediate state which usually appears after the peak of a possible outburst. If so, in future, this source may slow down its activities when the viscosity in this system is reduced as in any other outbursting source.

We would like to stress that CE computed by us counts soft photons from 0.1 keV to an upper energy limit automatically detected by our fitting method. If we concentrated on photons in the observed 2–40 keV range and counted the number of soft photons, we would have obtained a different, in fact, much higher CE. This is because we would have grossly underestimated number of soft photons. In Fig. 5, we show a comparison of CE computed by our method with ‘fracsctr’ obtained from *simpl* model (Steiner et al. 2011) for GX 339-4 data. *simpl* is an empirical model of Comptonization which computes fraction of photons from an input seed spectrum which are scattered into a power-law component. Fracsctr is fraction (in the scale up to 1.0) of input seed photons is Comptonized. Black and gray points are for the 2007 and 2010 outburst data respectively. Black stars and gray circles represent variations of fracsctr with CE when soft photons are taken from 0.1-40 keV CE(%) range. One generally sees that one increases with the other. From Fig. 5, we can see that fracsctr value varies around 0 to 0.8 this means 0-80 % photons are interacting with hot electron cloud. But if we compare with CE then only 0.005-0.35 % of photons are interacting with hot electron cloud which is more realistic. Computed CE values do support relative shape of CENBOL which is expected to intercept less than a few percent of soft photons from the Keplerian disk (Chakrabarti & Titarchuk 1995).

Another important issue is to correlate spectral and timing data. We mentioned that CE is higher for harder states. This is because location and height of shock wave are large. We have also mentioned that low frequency QPOs are due to oscillations of these shock waves and frequency is inverse of the infall time scale from post-shock region (Chakrabarti & Manickam 2000) till the inner sonic point. As such, larger shock radius means smaller QPO frequency, which is exactly what we observe! If we combine these results, then TCAF model would predict that CE would be larger when the QPO frequency is smaller and vice versa. In Fig. 6, we show measured QPO frequencies as a function of our CE for all the outbursts discussed in this paper. We find that CE is inversely correlated with QPO frequencies, although the relationship is not very tight in some cases. This could be because of presence of radio jets observed in all these outburst sources (Brocksopp et al. 2002; Casella et al. 2010; Corbel et al. 2010; Kalemci et al. 2005; Buxton & Bailyn 2004; Corbel & Tzioumis 2008; Migliari et al. 2007; Hjellming & Rupen 1995; Kaaret et al. 2003). While CE is influenced by electron clouds at base of a jet (post-shock region in TCAF solution), QPO frequency is not directly affected by the jet, but only by location of oscillating shock. This could be a primary reason why some outbursters do not show a tight correlation. However, this aspect requires further investigation.

It is also interesting to study variation of CE with luminosity in analogy with hardness ratio-intensity plots in the literature (Fender et al. 2004). Since hardness ratio is obtained from a fixed range of X-ray photons, independent of mass of black hole, it is difficult to interpret what a conventional colour-colour diagram really means. In Figs. 7a, and 7b, we plot CE vs. luminosity for both outbursts of XTE 1550-564 and GX 339-4 respectively. In Fig. 7(a), dark filled boxes represent variation of CE(%) with natural logarithm of luminosity in Eddington unit during 1998 outburst and gray filled circles represent same for 2000 outburst. In Fig. 7(b), black filled boxes represent 2007 outburst of GX 339-4, while gray filled circles represent the same for 2010 outburst of GX 339-4. For all plots, arrows of corresponding colour are provided to understand evolution of data during outbursts. Figures provide an idea about the relation between geometric size of the electron cloud and total

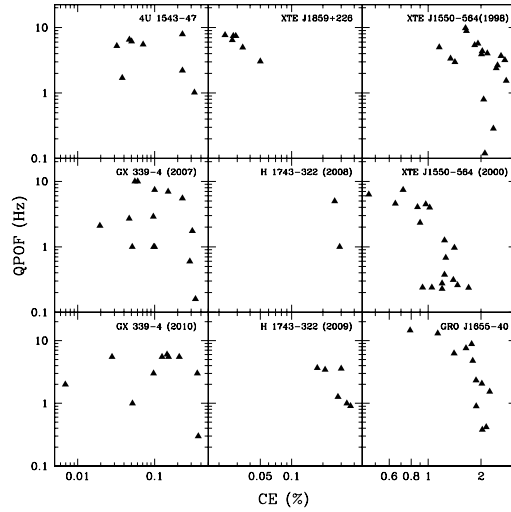


Figure 6. Variation of QPO frequency with CE(%) for all outbursts. The general trend is that the frequency increases as CE is decreased.

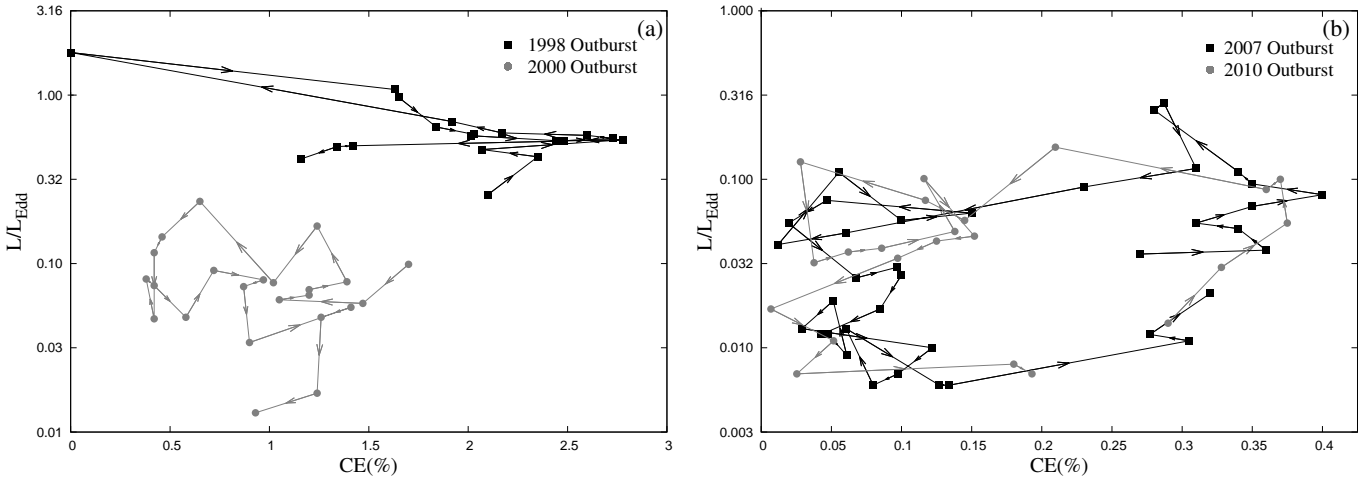


Figure 7. Variation of CE(%) with (L/L_{Edd}) for (a) 1998(black) and 2000(gray) outburst of XTE J1550-564, (b) 2007(black) and 2010(gray) outburst of GX 339-4.

luminosity during outburst. In case of XTE 1550-564 (Fig. 7a), we observe that both outbursts started and ended with high CEs, though final value of CE is lower than its initial value. However, this could be due to incompleteness of observation during onset of the outburst. Outburst of 2000 is clearly weaker and short lived. In both the cases, there is a hysteresis effect in that paths in rising and declining phases are not the same. This is expected, since formation time and disappearance time of a Keplerian disk by viscous effects are not identical (Giri & Chakrabarti 2013). In case of GX 339-4, both Figures are generally overlapping and thus both were of roughly equal strength. We note that CE is not necessarily highest at beginning or end in all these cases, though it is close to highest values achieved during outburst. This may be because CE is sensitive to the optical depth and not just physical size of the CENBOL. This is also the reason why QPO frequency variation (sensitive to the size of CENBOL) is not tightly correlated with CE. An important result is that CE of GX 339-4 is much lower as compared to that of XTE J1550-564. Since with spin the size of the CENBOL shrinks at least by a factor of two (Chakrabarti 1996), the degree of interception would also be reduced by the same factor. It is well known that spin of XTE J1550-564 is moderate (Steiner et al. 2011) while the spin of GX 339-4 is very high (Kolehmainen & Done 2010). It is possible that we are seeing effects of large spin in GX 339-4 in our calculation also.

In order to show that soft photons beyond dbb_e really do not contribute significantly, we recomputed the above values with soft photons till 40 keV. We do not find any significant difference in the result. So we believe that our results with dynamically obtained black body photon energy range yields sufficiently accurate results.

From the Table: 3, we see that range of CE is different for different objects. Duration of outbursts, QPO frequency range etc. are also found to be different. There is also a considerable scatter in CE which may be due to outflows from the CENBOL.

All these require a more thorough analysis for a unifying understanding of the outbursts. This will be addressed in our future publications. Another way to improve the result is to use TCAF model itself to fit the spectra and obtain blackbody energy range more accurately. A third, and more serious point is to consider spin of black hole which will reduce CE by virtue of smaller CENBOL size for higher spins. These aspects will be looked into in future.

7 ACKNOWLEDGMENT

We acknowledge the referee for his useful advice to improve the paper. PSP acknowledges SNBNCBS-PDRA Fellowship.

REFERENCES

- Axelsson, M., Borgonovo, L. & Larsson, S., *A&A*, 438, 999, 2005.
 Baily, C.D., Orosz, J.A. & Girard, T.M. et al., *Nature*, 374, 701, 1995.
 Belloni, T., Colombo, A. P. & Homan, J. et al., *A&A*, 390, 199, 2002.
 Belloni, T., *LNP*, 794, 53, 2010.
 Blissett, R.J., Pedersen, H. & Veron, M. et al., *IAU Circ*, 3858, 1, 1983.
 Brocksopp, C., Fender, R. P. & McCollough, M. et al., *MNRAS*, 331, 765, 2002
 Brocksopp, C., Jonker, P. G. & Maitra, D. et al., *MNRAS*, 404, 908-916, 2010
 Buxton, M. M. & Baily, C.D., *APJ*, 615, 880-886, 2004
 Campbell-Wilson, D., McTntyre, V., & Hunsted, R. W. et al., *IAU Circ*, 7010, 3, 1998
 Capitanio, F., Belloni, T. & Del Santo, M. et al., *MNRAS*, 398, 1194, 2009
 Casella, P., Maccarone, T. J. & O'Brien, K., et al., *MNRAS*, 404, 21, 2010
 Chaty, S., Haswell, C. A. & Malzac, J., et al., *MNRAS*, 346, 689, 2003
 Chakrabarti, S. K., *MNRAS* 283, 325, 1996.
 Chakrabarti, S. K. & Titarchuk, L. G., *APJ*, 455, 623, 1995.
 Chakrabarti, S. K. & Manickam, S. G., *APJ*, 531, 41, 2000.
 Chakrabarti, S. K., Nandi, A. & Manickam, S. G., et al., *APJ*, 579, 21, 2002.
 Chakrabarti, S. K., Debnath, D. & Nandi, A. et al., *A&A*, 489, 41, 2008.
 Chakrabarti, S. K., Dutta, B. G. & Pal, P. S., *MNRAS*, 394, 1463, 2009.
 Chen, Y. P., Zhang, S. & Torres, D. F., et al., *A&A*, 522, 99, 2010
 Chen, Tao, *IAU*, 275, 327, 2011
 Corbel, S., Kaaret, P. & Fender, R.P., et al., *APJ*, 632, 504, 2005.
 Corbel, S. & Tzioumis, A, *ATel*, 1349, 1, 2008.
 Corbel, S., Broderick, J. & Brocksopp, C., et al., *ATel*, 2525, 1, 2010.
 Coriat, M., Corbel, S. & Prat, L. et al., *MNRAS*, 416, 677, 2011.
 Corral-Santana, J. M., Casares, J. & Shahbaz, T., et al., *MNRAS*, 413, 15, 2011
 Das, S. & Chakrabarti, S.K., *IJMPD*, 13, 1955, 2004
 Debnath, D., Chakrabarti, S. K. & Nandi, A., *A&A*, 520, 98, 2010
 Del Santo, M., Belloni, T., & Homan, J. et al., *MNRAS*, 392, 992, 2009
 Dickey, J. M. & Lockman, F. J., *ARA&A*, 28, 215, 1990
 Doxsey, R., Bradt, H. & Fabbiano, G., et al., *IAU Circ.*, 3113, 1977
 Dutta, B. G. & Chakrabarti, S. K., *MNRAS*, 404, 2136, 2010
 Esin, A. A., McClintock, J. E. & Narayan, R., *ApJ*, 489, 865, 1997
 Fender, R., Belloni, T.E. & Gallo, E., *MNRAS*, 355, 1105, 2004
 Garcia, M. R., Brown, W. & Pahare, M. et al., *IAU Circ*, 7392, 2, 2000
 Gelino, D. M., Balman, S. & Kiziloglu, U. et al., *APJ*, 642, 438, 2006
 Giri, K. & Chakrabarti, S.K., *MNRAS*, 430, 2836, 2013
 Haardt F. & Maraschi L., *ApJ*, 380, L51, 1991
 Hannikainen, D. C., Wu, K. & Campbell-Wilson, D. et al., *ESASP*, 459, 291, 2001
 Hjellming, R. M. & Rupen, M. P., *Nature*, 375, 464, 1995
 Hunstead, R. W. & Webb, J., *IAU Circ*, 7925, 1, 2002
 Hynes, R. I., Mauche, C. W. & Haswell, C. A., et al., *APJ*, 539, 37, 2000
 Hynes, R. I., Steeghs, D. & Casares, J. et al., *APJ*, 583, 95, 2003
 Hynes, R. I., Haswell, C. A. & Cui, W. et al., *MNRAS*, 345, 292, 2003
 Hynes, R. I., Steeghs, D. & Casares, J. et al., *APJ*, 609, 317, 2004
 Hynes R. I., Robinson, E. L. & Pearson, K. J. et al., *APJ*, 651 401, 2006

- Jain, R. K., Bailyn, C. D. & Orosz, J. A. et al., APJ, 546, 1086, 2001
- Janiuk A., Czerny B., New Astron., 5, 7, 2000
- Jonker, P. G., Miller Jones J. & Homan J. et al., MNRAS, 401, 1255, 2010
- Kaaret, P., Corbel, S. & Tomsick, J. A., et al., APJ, 582, 945, 2003
- Kalemci, E., Tomsick, J. A. & Buxton, M. M. et al., APJ, 622, 508, 2005
- Kaluziński L. J. & Holt, S. S., IAU Circ, 3099, 1, 1977
- Kanbach, G., Straubmeier, C. & Spruit, H. C. et al., Nature, 414, 180, 2001
- Kato, S., PASJ, 57, 17, 2005
- Klein-Wolt, M., Fender, R. P. & Pooley, G. G., et al., MNRAS, 331, 745, 2002
- Kolehmainen, M. & Done, C., MNRAS, 406, 2206, 2010.
- Kong, A. K. H., Kuulkers, E. & Charls, P. A. et al., MNRAS, 311, 405, 2000
- Krimm, H. A., Barbier, L. & Barthelmy, S. D., et al., ATel, 968, 1, 2006
- Liu, B. F., Meyer, F. & Meyer-Hofmeister, E., A&A, 442, 555, 2005
- Makishima, K., Maejima, Y. & Mitsuda, K., et al., APJ, 308, 635, 1986
- Markert, T. H., Canizares, C. R. & Clark, G. W., et al., APJ, 184, 67, 1973
- Markwardt, C. B. & Swank, J. H., ATel, 414, 1, 2005
- Markoff, S., Falcke, H. & Fender, R., A&A, 372, 25, 2001
- Matilsky T. A., Giacconi, R. & Gursky, H. et al., APJ, 174, 53, 1972
- McClintock, J. E., Haswell, C. A. & Garcia, M. R., et al., APJ, 555, 477, 2001
- McClintock, J. E. & Remillard, R. A., CSXS.BOOK, 157, 2006
- McClintock, J. E., Remillard, R. A. & Rupen, P., et al., APJ, 698, 1398, 2009
- Mendez, M. & Van der Klis, M., APJ, 479, 926, 1997
- Merloni A., Fabian A. C., MNRAS, 321, 549, 2001
- Middleton, M., Done, C. & Gierlinski, M., et al., MNRAS, 373, 1004, 2006
- Migliari, S., Tomsick, J. A. & Markoff, S., et al., APJ, 670, 610, 2007
- Miller, J. M. & Remillard, R. A., IAU Circ, 7920, 2, 2002
- Morrison, R. & McCammon, D., ApJ, 270, 119, 1983
- Motta, S., Belloni, T. & Joman, J., MNRAS, 400, 1603, 2009
- Muno, M. P., Morgan, E. H. & Remillard, R. A., APJ, 527, 321, 1999
- Nandi, A., Debnath, D., Mandal, S. & Chakrabarti, S. K., A&A, 542, 56, 2012
- Neilsen, J., Remillard, R. A. & Lee, J. C., APJ, 737, 69, 2011
- Orosz, J. A. & Bailyn, C. D., APJ, 477, 876, 1997
- Orosz, J. A., Jain, R. K. & Bailyn, C. D. et al., APJ, 499, 375, 1998
- Orosz, J. A., Bailyn, C. D. & Jain, R. K., IAU Circ, 7009, 1, 1998
- Orosz, J. A., Groot, P. J. & Van der Klis, M. et al., APJ, 568, 845, 2002
- Ohsuga, K., Kato, Y. & Mineshige, S., APJ, 627, 782, 2005
- Pal, P. S., Chakrabarti, S. K. & Nandi, A., IJMPD, 20, 2281, 2011
- Pal, P. S., Chakrabarti, S. K. & Nandi, A., AdSpR, 52, 740, 2013
- Park, S., Miller, J. M. & McClintock, J. E. et al., APJ, 610, 378, 2004
- Pooley, G. G., ATel, 385, 1, 2005
- Rao, A. R., Yadav, J. S. & Paul, B., APJ, 544, 434, 2000a
- Reig, P., Papadakis, I. E. & Shradar, C. R. et al., APJ, 644, 424, 2006
- Remillard, R., Morgan, E. & Smith, D. et al., IAU Circ, 7389, 2, 2000
- Remillard, R., Muno, M. P. & McClintock, J. E. et al., APJ, 580, 1030, 2002
- Remillard, R., Garcia, M. & Torres, M. A. P. et al., ATel, 384, 1, 2005
- Revnivtsev M., Chernyakova, M. & Capitanio, F. et al., ATel, 132, 1, 2003
- Rupen M, P, Mioduszewski, A.J. & Dhawan, V., ATel, 142, 1, 2003
- Rupen M. P., Dhawan, V. & Mioduszewski, A. J., ATel, 609, 1, 2005
- Rutledge, R., Fox, D. & Smith, D. A., ATel, 37, 1, 1998
- Shaposhnikov, N., Swank, J. & Shrader, C. R. et al., APJ, 655, 434, 2007
- Smith, D. A., IAU Circ, 7008, 1, 1998
- Smith, D. A., ATel, 47, 1, 1999
- Sobczak, G. J., McClintock, J. E. & Remillard, R. A. et al., APJ, 517, 121, 1999a
- Sobczak, G. J., McClintock, J. E. & Remillard, R. A. et al., APJ, 520, 776, 1999b
- Steiner, J. F., Reis, R. C. & McClintock, J. E. et al., MNRAS, 416, 941, 2011
- Swank J., ATel, 301, 1, 2004
- Sunyaev, R. A. & Titarchuk, L. G, A&A, 143, 374, 1985

- Taam, R. E., Chen, X. & Swank, J. H., APJ, 485, 83 , 1997
Tanaka, Y. & Lewin, W. H. G., xrb.nasa, 126, 1995
Titarchuk, L. G., APJ, 434, 570, 1994
Tomsick, J. A., Corbel, S. & Kaaret, P., APJ, 563, 229, 2001a
Vadawale, S. V., Rao, A. R. & Chakrabarti, S. K., A&A, 372, 793, 2001
Van der Hooft, F., Heemskerk, M. H. M., & Alberts, F., et al., A&A, 329, 538, 1998
Wandel A. & Liang E. P., ApJ, 380, 84, 1991
White N. E. & Marshall F. E., IAU Circ., 3806, 2, 1983
Wilson, C. A., Harmon, B. A. & Paciesas, W. S. et al., IAU Circ, 7010, 2, 1998
Wood, A., Smith, D. A. & Marshall, F. E., et al., IAU Circ., 7274, 1, 1999
Yamaoka, K., Sugizaki, M. & Nakahira, S., et al., ATel, 2380, 1, 2010
Yuan, F., Cui, W. & Narayan, R., APJ, 620, 905-914, 2005
Zdziarski A. A., Lubinski P. & Gilfanov M. et al., MNRAS, 342, 355, 2003
Zhang, S. N., Wilson, C. A. & Harmon, B. A. et al., IAU Circ., 6046, 1, 1994
Zhang, S. N., Ebisawa, K. & Sunyaev, R. et al., APJ, 479, 381, 1997
Zurita, C., Sanchez-Fernandez, C., & Casares, J. et al., MNRAS, 334, 999, 2002
Zurita, C., Rodriguez, D. & Rodriguez-Gil, P. et al., ATel, 383, 1, 2005a
Zurita, C., Casares, J. & Muoz-Darias, T. et al., ATel, 428, 1, 2005b
Zurita, C., Torres, M. A. P. & Steeghs, D. et al., APJ, 644, 432, 2006